RSC Advances

ROYAL SOCIETY OF CHEMISTRY

www.rsc.org/advances

Journal Name

RSCPublishing

COMMUNICATION

One-step chemical vapor deposition approach for solid solution $Pr_xNd_{1-x}B_6$ nanowires growth

Cite this: DOI: 10.1039/xoxxoooooox

Qidong Li, Yanming Zhao*, Qinghua Fan, Wei Han

Received ooth January 2012,
Accepted ooth January 2012

DOI: 10.1039/xoxxoooooox

www.rsc.org/

Dual-rare earth hexaborides $Pr_xNd_{1-x}B_6$ nanowires have been successfully synthesized on silicon substrates by one-step CVD method at the temperature of 1030 ºC. The quasi-aligned nanowires are shown to be structurally uniform and well-doped single crystals based on the comprehensive analysis. The present preparation technique is an effective and invaluable method to develop and optimize dual-REB_6 nanostructured emitters.

Rare earth hexaborides (REB_6) has been investigated and applied as both thermionic and field electron emitter cathode materials in various vacuum electronic devices in past decades, as their brilliant set of properties such as low work function, high chemical stability, low vapor pressure and high melting point offer them high brightness and long service life.[1] In the context of field emission (FE), in which electrons are emitted from a material's surface into vacuum by tunneling through a potential barrier under a high electric field,[2] one-dimensional (1-D) nanostructures are seemed to be the preferred forms due to their large enhancement factor originated from high aspect ratio according to the typical Fowler-Nordheim (F-N) theory.[3] As a consequence, various types of REB_6 nanoforms, i.e. nanowires,[4] nanoneedles,[5] nanorods,[6] nanotubes,[7] nanoawls,[8] etc. have been fabricated and applied as electron emitters. Doping is a well-know and efficient means to tune the property of a material by compositional and morphological variation.[9-10] Since the isostructural nature of REB_6 family,[11] dual-rare earth hexaborides solid solutions are possible to form. And the dual-REB_6 might supply a relatively high current at a lower temperature in comparison with individual-cation ones.[11] According to our previously reported $La_xNd_{1-x}B_6$ nanowires,[12] dual-REB_6 tended to form smoother and higher aspect ratio nanowires benefited from the lower melting point of dual-RE eutectic alloy formed during growth. The FE performance was improved effectively compared with both LaB_6 and NdB_6. We hope the same would hold true in praseodymium-mixed NdB_6. Herein, $Pr_xNd_{1-x}B_6$ nanowires are synthesized through a gas-solid reaction system in the current work and comprehensive characterization have been demonstrated to understand the morphology, structure and composition of these nanowires, attempting to provide clues of structure-property relationship for dual-REB_6 emitters.

Starting materials of praseodymium, neodymium metal powders and BCl_3 gas were used as received. $Pr_xNd_{1-x}B_6$ nanowires were fabricated using a chemical vapor deposition (CVD) method following the reaction below:
xPr(g) + (1-x)Nd(g) + $6BCl_3$(g) + $9H_2$(g) = $Pr_xNd_{1-x}B_6$(s) + 18HCl(g). Fig. 1 shows the schematic illustration of rare earth metals and instruments used for the preparation of the solid solution nanowires. In a typical process, nearly same amount of Pr and Nd were mixed uniformly and evenly distributed onto Si (100) wafers (1cmx1cm in size) in the center of a quartz tube. After being evacuated and flushed with inlet gases (30% H_2+70% Ar in volume percentage) several minutes, the furnace was heated from room temperature to 1030 ºC at a rising rate of 15 ºC min^{-1} under a ~30 sccm gas flow. The samples were held at 1030 ºC for 30 min, and the BCl_3 gas was introduced during the preservation process at a rate of 20 sccm. Subsequently, the furnace was cooled down to room temperature. The as-obtained samples were immersed into hydrochloric acid solution and double distilled water to remove the unwanted by-products. Then the substrates were dried in an oven at 80 ºC for 2h. Typical products in gray colour were finally acquired. The whole fabrication procedures were conducted in atmospheric pressure without vacuum-pumping.

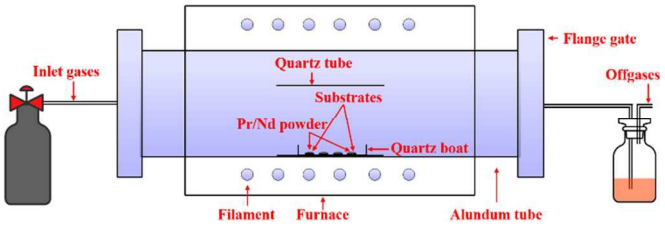

Fig. 1 The schematic illustration of experimental set-up for $Pr_xNd_{1-x}B_6$ nanowire growth.

Fig. 2(a) shows a typical XRD pattern of the as-synthesized product, obtained by using a TD3500 X-ray diffractometer equipped with Cu Kα radiation (XRD, λ=1.5419Å), indicating the formation of $Pr_xNd_{1-x}B_6$ phase. The standard PrB_6 and NdB_6 are presented below. The similar peaks positions of PrB_6 and NdB_6 should be attributed to the isostructural REB_6 (space group: *Pm-3m*) and nearly same size of Pr (radius=2.67 Å) and Nd (radius=2.64 Å) atoms. One can see that all

experimental peaks could be assigned without any extra impurity peaks in the spectrum, confirming the highly pure phase of $Pr_xNd_{1-x}B_6$. The relatively stronger (100) peak of $Pr_xNd_{1-x}B_6$ product, which differs from the standard ones, reveals their anisotropy nature and preferred oriented direction along [100] crystal direction. Preliminary *Rietveld* refinement were performed to further illustrate the cell parameter of the obtained sample (Fig. 2b). The resulted lattice constant of 4.127(8) Å, which is nearly same as that of PrB_6 and NdB_6, indicating the successful formation of solid solution $Pr_xNd_{1-x}B_6$ phase.

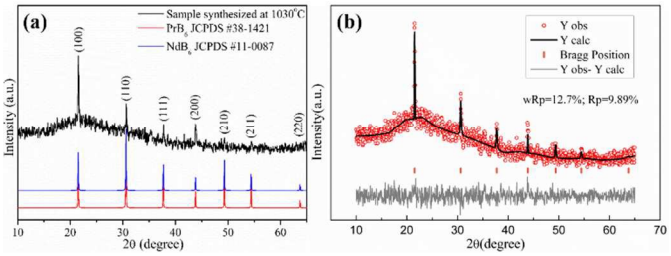

Fig. 2 (a)XRD pattern of the as-synthesized $Pr_xNd_{1-x}B_6$ sample. (b) *Rietveld* analysis of the sample.

The representative surface topographies of as-obtained $Pr_xNd_{1-x}B_6$ nanowires are presented in Fig. 3(a-c) with different magnifications under the operation of a field-emission scanning electron microscope (FE-SEM, Navo NanoSEM430). A uniformly distributed nanowires can be found in Fig. 3(a), with smooth surfaces devoid of any adherent particles or impurities. The quasi-aligned forms of nanowires in Fig. 3(b) demonstrate that the $Pr_xNd_{1-x}B_6$ nanowires are around 150nm in diameter and length extending to more than a few micrometers. Fig. 3(c) shows the high-resolution mode of SEM image, from which we can see the evenly distributed nanowires with uniform dimensions across their entire length. The relatively high aspect ratio is beneficial for the field emission performance.[3]

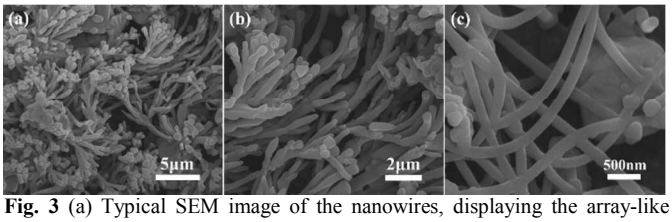

Fig. 3 (a) Typical SEM image of the nanowires, displaying the array-like nanostructures. (b) Medium-magnification image of $Pr_xNd_{1-x}B_6$ nanowires with quasi-aligned features. (c) High-magnification image of the nanowires.

To understand the structural aspects, detailed analysis was performed using a transmission electron microscope (TEM, Tecnai™ G^2 F30). Fig. 4(a-c) with different magnifications were rotated to display the dimensional feature of the individual $Pr_xNd_{1-x}B_6$ nanowire. The smooth defect-free surface and tip without attached droplet can be observed, which is consistent with our catalyst-free experiment condition. The amorphous matter in lower contrast areas of Fig. 4a is due to the decomposed of Si surfaces corroded by BCl_3 gas, and was scraped onto copper grid when applied for TEM characterization. We can also find thin amorphous shell coated on the surface of nanowire from Fig 4b-c. Xu *et al.* hold the point that the shells should be attributed to the deposition of boron species on the surfaces of rare earth metals and then prevent the localized vaporization of metals, thus at the same time producing amorphous boron surrounding the nanowires since this is the only feasible amorphous phase among the three elements (Pr, Nd, B).[13] The amorphous boron shells had also been ascertained by Zhang *et al.* though electron energy loss spectrum (EELS) detection.[14] It can also be seen from Fig. 4(c), which was acquired by rotated the view of Fig. 4b clockwise and is the magnification of the red circled area of Fig. 4b, that the growth of the nanowire is terminated by three different lattice planes that are labeled with letters D, E and F on the image. The high-resolution (HR) TEM images characterizing these faceted lattice planes are displayed in Fig. 4(d-e) in corresponding sequence. Fig 4(d) shows the area marked with letter D in Fig. 4(c), whose surface is indexed to be terminated with the (320) lattice plane. The nanowire tip is presented in Fig. 4(e) (labeled E in Fig. 4(c)), from which the interplanar fringes can be clearly observed, and the d-spacing between two set of fringes is ~0.26nm, agreeing with the (111) crystal faces. F-N theory indicates the merit of aspect ratio on FE property of an emitter, suggesting the importance of the nanowire tip which serves as main emission sites upon high electric field. The higher stability of (111) crystal planes may upgrade the performance during electron emission process.[15] Another series of lattice fringes can also be indicated along the axial direction of the nanowire in Fig. 4(e), the 0.41nm d-spacing correspond to (100) plane of REB_6 and perpendicular ones can be attributed to (110) crystal plane with a d-spacing of ~0.29nm, which indicate the axial direction is [110], that is the growth direction of the nanowire. Another segment (Fig. 4(f)), marked with letter F in Fig. 4(c), shows a (210) facet. Fig. 4(g) is the corresponding SAED pattern, which agrees well with HRTEM results. It is identical over the entire nanowire, confirming its single-crystalline nature.

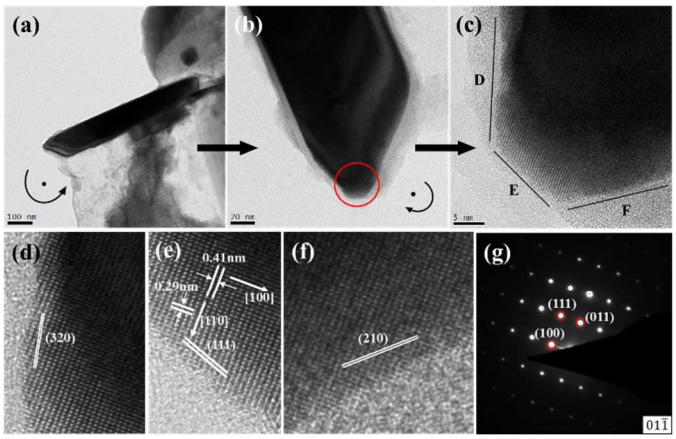

Fig. 4 TEM images of the $Pr_xNd_{1-x}B_6$ samples. (a-b) Typical TEM images. (c) HRTEM image of the nanowire tip with terminated facets labeled with letters D, E and F. (d-f) Magnified lattice images of D-F, respectively. (g) The corresponding SAED pattern.

Detailed chemical analysis were carried out using elemental mapping, EELS and EDS. Fig. 5(a) shows a typical TEM image of a single nanowire and the corresponding elemental maps, demonstrating that Nd and Pr are homogeneously distributed within the individual nanowire. EELS technique was applied to confirm the chemical composition of the nanowire. As shown in Fig. 5(b) (acquired from the area in red circle of Fig. 5(a)), no other impurities are detected except the boron element characteristic K-shell ionization edge (≈188 eV) signals. The results shows the successful synthesis of borides products. A representative X-ray energy dispersive spectrometer (EDS) image taken from the FE-SEM attachment is demonstrated in Fig. 5(c) with quantitative analysis in the table inset. We can find the signals of O, Nd, Pr, Si and Cl, with their specific atomic and weight percentage shown in the table. The nearly same atomic percentage of Nd and Pr are in consistent with the initial set of starting materials. Oxygen signal may come from the slight oxidation of Nd and Pr powders before putting them into the tubular furnace.[16] The Si substrate used to load the growth of

nanowires should be the reason of appearance of Si peak in the spectrum. The Cl signal observed is probably from the decomposition and migration of the BCl_3 raw material. On the basis of these experiment results, the as-synthesized products are found to be single-crystalline $Pr_xNd_{1-x}B_6$ nanowires with [110] growth direction.

Unlike the conventional vapor-liquid-solid (VLS) mechanism proposed for nanostructures growth, from which one can find nanosized catalyst particles at the tips of the nanowires, [17] the growth method of $Pr_xNd_{1-x}B_6$ nanowires in this vapor deposition system should be attributed to a dominant VLS-like mechanism with a self-catalytic growth mechanism like our recent work of $La_xNd_{1-x}B_6$.[12] That is to say, the melting Pr-Nd alloy and vapor serve as reactants and catalysts simultaneously during the growth process. One thing to be highly noted is that the vapor-solid (VS) mechanism[18] can be unambiguously ruled out in the present system on account of the vapor (provided by pyrolysis of BCl_3 and Pr/Nd vapor), liquid (supplied by melting Pr-Nd alloy), and solid (realized by formation of $Pr_xNd_{1-x}B_6$ nanowires) involved throughout the growth procedure. We have also designed a simple experiment to certify the vapor, liquid and solid phase. Detailed information can be found in ESI.

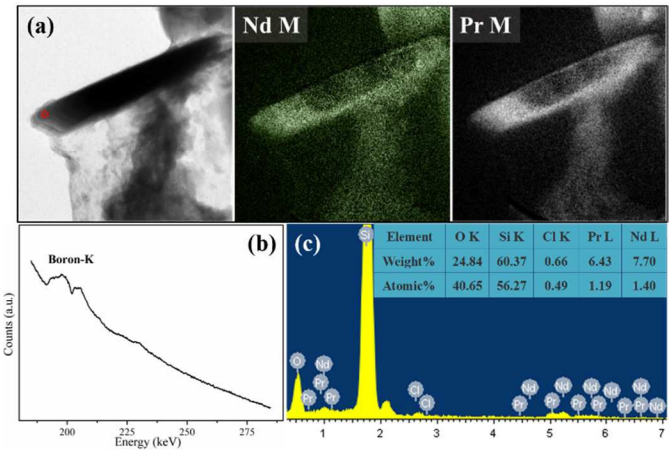

Fig. 5 (a) TEM image and the corresponding elemental maps of Nd and Pr. (b) EELS spectrum acquired from the red circled area of individual $Pr_xNd_{1-x}B_6$ nanowire in (a). (c) EDS results, inset shows the quantitative analysis.

Conclusions

We demonstrate the effective fabrication of $Pr_xNd_{1-x}B_6$ nanowires by using a one-step gas-solid reacting CVD approach. The preparation technique is an effective and invaluable method to develop and optimize dual-REB_6 nanostructured emitters. The well-characterized morphology of the nanowires are quasi-aligned arrays with smooth surfaces and have diameters around 150nm and lengths extending to more than a few micrometers. The HRTEM results clearly reveal their single crystalline nature, having terminated facets of indices as (320), (111) and (210), and the growth direction of the nanowires is its [110] lattice direction. The formation of these nanowires is as per the dominant VLS-like mechanism with a self-catalytic growth mechanism and has been explained on the basis of the starting materials together with the SEM and TEM images. The $Pr_xNd_{1-x}B_6$ nanowires' potential applications include providing emitters of electrons for TEM, SEM, flat panel displays, as well as other nanoelectronic building blocks.

Acknowledgements

This work was funded by NSFC Grant (No. 51372089, 51172077, 51373205) supported through NSFC Committee of China, and the Foundation of (No. 2014ZB0014) supported through the Fundamental Research Funds for the Central Universities.

Notes and references

State Key Laboratory of Luminescent Materials and Devices, South China University of Technology, Guangzhou, 510641, P. R. China.
**Corresponding author. E-mail: zhaoym@scut.edu.cn*

Electronic Supplementary Information (ESI) available: [details of any supplementary information available should be included here]. See DOI: 10.1039/c000000x/

1 M. Gesley and L. Swanson, *Surf. Sci.*, 1984, **146**, 583.
2 R. Gomer, *Field emission and Field Ionization*, Harvard University Press, Cambridge, Mass., 1961.
3 R. H. Fowler and L. W. Nordheim, *Proc. R. Soc. London, Ser. A*, 1928, **119**, 173.
4 H. Zhang, Q. Zhang, J. Tang and L.-C. Qin, *J. Am. Chem. Soc.*, 2005, **127**, 2862.
5 J. Q. Xu, G. H. Hou, T. Mori, H. Q. Li, Y. R. Wang, Y. Y. Chang, Y. S. Luo, Y. B. Yu, Y. Ma and T. Y. Zhai, *Adv. Funct. Mater.*, 2013, **23**, 5038.
6 M. Jha, R. Patra, S. Ghosh and A.K. Ganguli, *J. Mater. Chem.*, 2012, **22**, 6356.
7 M.F. Chi, Y.M. Zhao, Q.H. Fan and W. Han, *Ceram. Int.*, 2014, **40**, 8921.
8 W. Han, H. Zhang, J. Chen, Y.M. Zhao, Q.H. Fan and Q.D. Li, *RSC Adv.*, 2015, **5**, 12605.
9 Q. Wu, N. Liu, Y.L. Zhang, W.J. Qian, X.Z. Wang and Z. Hu, *J. Mater. Chem. C.* 2015. **3**. 1113.
10 L.H. Bao, L.M. Chao, W. Wei and O. Tegus, *Mater. Lett.*, 2015, **139**, 187-190.
11 S.L. Zhou, J.X. Zhang, L.H. Bao, X.G. Yu, Q.L. Hu and D.Q. Hu, *J. Alloys Compd.*, 2014, **611**, 130.
12 Q.D. Li, H. Zhang, J. Chen, Y.M. Zhao, W. Han, Q.H. Fan, Z.Y. Liang, X.D. Liu and Q. Kuang, *J. Mater. Chem. C.* 2015, **3**, 7476.
13 T. T. Xu, J. G. Zheng, A. W. Nicholls, S. Stankovich, R. D. Piner and R. S. Ruoff, *Nano Lett.*, 2004, **4**, 2051.
14 H. Zhang, J. Tang, Q. Zhang, G. Zhao, G. Yang, J. Zhang, O. Zhou and L.-C. Qin, *Adv. Mater.*, 2006, **18**, 87.
15 T. Takigawa, I. Sasaki, T. Meguro and K. Motoyama, *J. Appl. Phys.*, 1982, **53**, 5891.
16 J.Q. Xu, Y.M. Zhao, C.Y. Zou and Q.W. Ding, *J. Solid State Chem.*, 2007, **180**, 2577.
17 R.S. Wagner and W.C. Ellis, *Appl. Phys. Lett.*, 1964, **4**, 89.
18 G.W. Sears, *Acta Metall.*, 1955, **3**, 367-367.